Activity-induced instability of phonons in 1D microfluidic crystals

Alan Cheng Hou Tsang, Michael Shelley, and Eva Kanso*

January 2, 2018

1 Sphere moving in Hele-Shaw confinement

Consider a sphere of radius R moving with velocity $\mathbf{U}$ in an unbounded domain of viscous fluid. The velocity field produced by the sphere is given by (see, e.g., [1, Chapter 3, §3.3.1])

$$\mathbf{u}(\mathbf{r}) = 6\pi\eta R\mathbf{U}\cdot\frac{1}{8\pi\eta}\left[\left(\frac{\mathbf{I}}{r}+\frac{\mathbf{r}\otimes\mathbf{r}}{r^3}\right)+\frac{R^2}{6}\left(\frac{2\mathbf{I}}{r^3}-\frac{6\mathbf{r}\otimes\mathbf{r}}{r^5}\right)\right], \tag{1}$$

where η is the fluid viscosity, $\mathbf{r}$ is a position vector measured from the center of the sphere and $r = \|\mathbf{r}\|$. Also, $\mathbf{I}$ is the identity matrix and the symbol $\otimes$ denotes the outer product. The first term on the right-hand side corresponds to a Stokeslet (a fundamental singularity of the Stokes equations) while the second term corresponds to a source dipole. Note that the source dipole is a potential flow solution to the Stokes equations and can be written as the Laplacian of the Stokeslet: $\left(2\mathbf{I}/r^3 - 6\mathbf{r}\otimes\mathbf{r}/r^5\right) = \nabla^2\left(\mathbf{I}/r + \mathbf{r}\otimes\mathbf{r}/r^3\right)$; see, e.g., [1, chapter 2].

We constrain the spherical particle to move in *Hele-Shaw* confinement, where h is the separation distance between the two flat plates bounding the *Hele-Shaw* cell and $R \ll h$, see Fig. 1 of the main text. By linearity of the Stokes equations, we immediately obtain that the velocity field produced by a confined spherical particle is the sum of the velocity fields of a confined Stokeslet and a confined potential dipole. A detailed calculation of the velocity field of a Stokelest confined between two parallel walls can be found in [2]. Liron and Mochon showed that in the far-field, for $r \gg h$, a Stokeslet perpendicular to the confining walls induces an exponentially decaying velocity field; a Stokeslet parallel to the walls induces an exponentially decaying velocity in the direction perpendicular to the confining walls but its far-field flow in the direction parallel to the confining walls is that of a two-dimensional source dipole. The direction of the source dipole is in the same direction as the original Stokeslet and its strength depends in a parabolic way on its placement between the two walls. Mathematically, for a Stokeslet of unit strength pointing in the horizontal direction given by $\mathbf{e} = \mathbf{U}/\|\mathbf{U}\|$ and located in a plane $z = \delta$ ($|\delta| < h/2$) between the two walls, one has (see [2, equation (51)])

$$\mathbf{u}^{\text{3D}}_{\text{stokeslet}} = \frac{1}{8\pi\eta}\left(\frac{\mathbf{I}}{r}+\frac{\mathbf{r}\otimes\mathbf{r}}{r^3}\right)\cdot\mathbf{e} \quad\Longrightarrow\quad \mathbf{u}^{\text{2D}}_{\text{stokeslet}} \approx -\frac{3h}{2\pi\eta}\left(\frac{1}{4}-\frac{\delta^2}{h^2}\right)\left(\frac{1}{4}-\frac{z^2}{h^2}\right)\left(\frac{\mathbf{I}}{\|\mathbf{x}\|^2}-2\frac{\mathbf{x}\otimes\mathbf{x}}{\|\mathbf{x}\|^4}\right)\cdot\mathbf{e}, \tag{2}$$

where $\mathbf{x} = x\mathbf{e}_1 + y\mathbf{e}_2$ is the planar position vector and $(\mathbf{e}_1, \mathbf{e}_2)$ is an inertial frame in the (x, y)-plane. The contribution of the source dipole in confinement can be obtained by rewriting it in the unconfined domain as the Laplacian of a Stokeslet, then applying (2) to get (see [3] for more details)

$$\mathbf{u}^{\text{3D}}_{\text{source dipole}} = \frac{1}{8\pi\eta}\boldsymbol{\nabla}^2\left(\frac{\mathbf{I}}{r}+\frac{\mathbf{r}\otimes\mathbf{r}}{r^3}\right)\cdot\mathbf{e} \quad\Longrightarrow\quad \mathbf{u}^{\text{2D}}_{\text{source dipole}} \approx \frac{3}{\pi\eta h}\left(\frac{1}{4}-\frac{\delta^2}{h^2}\right)\left(\frac{\mathbf{I}}{\|\mathbf{x}\|^2}-2\frac{\mathbf{x}\otimes\mathbf{x}}{\|\mathbf{x}\|^4}\right)\cdot\mathbf{e}. \tag{3}$$

Taken together, (2) and (3) imply that the leading order term in the velocity field produced by sphere moving between two walls is given by a dipole of the form

$$\mathbf{u}(\mathbf{x}) = -\mathbf{D}\cdot\left(\frac{\mathbf{I}}{\|\mathbf{x}\|^2}-2\frac{\mathbf{x}\otimes\mathbf{x}}{\|\mathbf{x}\|^4}\right), \tag{4}$$

*Kanso@usc.edu

where $\mathbf{D}$ is a vector quantity encoding the strength and direction of the dipole. If the sphere is located at $\delta = 0$ and the velocity is to be evaluated in the same plane $z = 0$, one gets

$$\mathbf{D} = \frac{3}{8\pi\eta}\left(\frac{h}{4} - \frac{R^2}{3h}\right)(6\pi\eta RU\mathbf{e}) = \frac{3}{16}R\left(\frac{3h^2 - 4R^2}{h}\right)U\mathbf{e} \tag{5}$$

We rewrite (4) in component form where $\mathbf{x} \equiv (x, y)$, $\mathbf{u} \equiv (u_x, u_y)$ and $\mathbf{D} \equiv (D_x, D_y)$.

$$\begin{pmatrix} u_x \\ u_y \end{pmatrix} = -\begin{pmatrix} -x^2 + y^2 & -2xy \\ -2xy & x^2 - y^2 \end{pmatrix}\begin{pmatrix} D_x \\ D_y \end{pmatrix} = \begin{pmatrix} D_x(x^2 - y^2) + 2D_y xy \\ 2D_x xy - D_y(x^2 - y^2) \end{pmatrix}. \tag{6}$$

To conclude this section, we rewrite the dipolar velocity field in complex notation,

$$\bar{u} = u_x - \mathrm{i}u_y = \frac{\sigma}{z^2} = \frac{\rho^2 U e^{i\alpha}}{z^2}, \tag{7}$$

where $z = x + \mathrm{i}y$ and $\sigma = D_x + \mathrm{i}D_y$. One can readily verify after straightforward calculation that the expressions for u_x and u_y given by (7) are identical to those in (6) for $\sigma = \rho^2 U e^{i\alpha}$, where α is the angle between $\mathbf{U}$ and the x-axis and $\rho^2 = (3h^2 - 4R^2)3R/16h$, where ρ is an effective radius corresponding to a planar disc that produces the same dipolar flow as the confined sphere.

2 Confined microswimmer: dumbbell model

In Section 1, we established that the far-field flow produced by the motion of a sphere in *Hele-Shaw* confinement is that of a potential dipole of strength $\sigma = \rho^2 U e^{i\alpha}$, where ρ is the effective radius of the sphere and α is the direction of its heading. We now consider a confined microswimmer, also referred to as an *active particle*, composed of two connected spheres of radii R_1 and R_2 located at z_1 and z_2, respectively, and connected by a frictionless rod of length $l \gg R_1, R_2$. Let z_o and α_o denote, respectively, the hydrodynamic center of the microswimmer and its orientation in the (x, y) plane. Following [4] and [5, §3.3], the equations governing the translational and rotational motion of the dumbbell system are obtained by writing the sum of forces for each sphere separately, expanding the velocity about the hydrodynamic center of the two-spheres, and rearranging terms to get

$$\begin{aligned} \dot{\bar{z}}_o &= U_o e^{-\mathrm{i}\alpha_o} + \mu\bar{w}(z_o), \\ \dot{\alpha}_o &= \mathrm{Re}\left[\nu_1 \frac{d\bar{w}}{dz}\mathrm{i}e^{2\mathrm{i}\alpha_o} + \nu_2\bar{w}\mathrm{i}e^{\mathrm{i}\alpha_o}\right]. \end{aligned} \tag{8}$$

Here, U_o is the self-propelled speed of the dumbbell particle and $w(z)$ is the velocity field of the ambient fluid. The overline notation denotes the complex conjugate: $\bar{z}_o$ is the complex conjugate of z_o and $\bar{w}$ is the complex conjugate of w. The coefficient μ is a lumped translational motility coefficient, and ν_1 and ν_2 are lumped rotational motiliy coefficients. In the following, we ignore the rotational response to flow gradient $d\bar{w}/dz$ because it is of higher order in comparison to the rotational response to $\bar{w}$ itself (see [4] and [5]) and we set $\nu_2 = \nu$. The sign of ν dictates how the swimmer orients in local flow: for a large tail swimmer ($R_2 > R_1$), one gets $\nu > 0$ and the swimmer tends to align with the local flow, whereas for a large head swimmer, $\nu < 0$ and the swimmer aligns opposite to the local flow.

3 1D lattice of microswimmers: problem formulation

Equations of motion. We apply (8) to study the interaction of an infinite one-dimensional array of confined microswimmers subject to a uniform background flow of speed V. The resulting equations of motion are listed as equations (1) in the main text and reproduced here for convenience,

$$\begin{aligned} \dot{\overline{z}}_n &= U\mathrm{e}^{-\mathrm{i}\alpha_n} + \mu V + \mu\overline{w}(z_n), \\ \dot{\alpha}_n &= \nu\mathrm{Re}\left[(V + \overline{w})\mathrm{i}\mathrm{e}^{\mathrm{i}\alpha_n}\right]. \end{aligned} \tag{9}$$

The conjugate velocity due to hydrodynamic coupling between the particles is given by

$$\overline{w}(z) = \sum_{m=-\infty}^{\infty} \frac{\sigma_m}{(z - z_m)^2}, \tag{10}$$

where $\sigma_m = a^2[U\mathrm{e}^{\mathrm{i}\alpha_m} - (1-\mu)V]$ is the dipole strength. It is useful for the discrete particle simulations as well as the linear stability analysis to represent the infinite crystal as a periodic lattice of N active particles with spatial periodicity L that is an integer multiple of d; see Fig. 1. The conjugate velocity (10) becomes

$$\overline{w}(z) = \left(\frac{\pi}{L}\right)^2 \sum_{m=1}^{N} \sigma_m \csc^2\left[\frac{\pi}{L}(z - z_m)\right]. \tag{11}$$

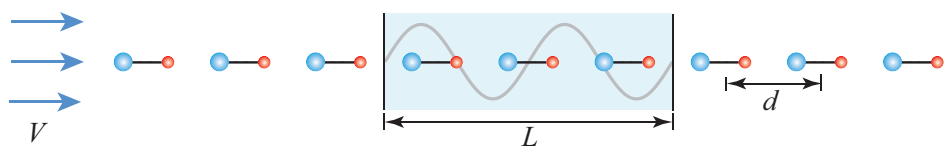

Figure 1: *Schematic of a 1D active crystal.*

Lattice configuration. The lattice configuration $z_n - z_m = md$ and $\alpha_n = 0$ is an equilibrium solution of (9), for which all active particles move at the same velocity $U + \mu(V + u)$,

$$\dot{\overline{z}}_n\big|_{\text{lattice}} = U + \mu(V + u), \qquad \dot{\alpha}_n\big|_{\text{lattice}} = 0. \tag{12}$$

Here, u is the lattice velocity arising from hydrodynamic interactions among the active particles

$$u = \sum_{m=-\infty}^{\infty} \frac{\sigma}{(md)^2} = \sum_{m=1}^{\infty} \frac{2\sigma}{(md)^2} = \frac{\pi^2\sigma}{3d^2}. \tag{13}$$

Linearized equations about lattice configuration. Consider a small perturbation of the lattice, $z_n = z_n|_{\text{lattice}} + \delta z_n$, where $(z_n - z_m)_{\text{lattice}} = md$ and $\alpha_n \equiv \delta\alpha_n$. The linearized equations of motion are given in (3) in the main text and reproduced here for convenience,

$$\begin{aligned} \frac{d(\overline{\delta z}_n)}{dt} &= -U\mathrm{i}\delta\alpha_n - \mu \sum_{m=-\infty}^{\infty} \frac{2\sigma(\delta z_n - \delta z_m)}{(md)^3}, \\ \frac{d(\delta\alpha_n)}{dt} &= -\nu(V + u)\delta\alpha_n - \nu\mathrm{Re}\left[\mathrm{i} \sum_{m=-\infty}^{\infty} \frac{2\sigma(\delta z_n - \delta z_m)}{(md)^3}\right]. \end{aligned} \tag{14}$$

where the dipole strength $\sigma_m \approx \sigma = a^2[U - (1-\mu)V]$ is constant. The perturbations $(\delta z_n, \delta\alpha_n)$ evolve in a frame of reference moving with the lattice with speed $U + \mu(V + u)$.

4 Plane Wave Perturbations

Plane wave perturbations. Consider plane wave perturbations, $\delta z_n = C(\mathrm{e}^{\mathrm{j}(knd - \omega t)}$, where $C = A$ for longitudinal waves and $C = \mathrm{i}B$ for transverse waves. Here, $(\mathrm{j}^2 = -1)$ is the imaginary unit in the wave complex plane, k is the perturbation wavenumber and ω is the perturbation frequency. The parameters A and B correspond to the longitudinal and transverse amplitudes of the perturbation.

Closed-form expression of the infinite sum. We substitute $\delta z_n = C\mathrm{e}^{\mathrm{j}(knd-\omega t)}$ into the infinite in (14) and assume $|C| \ll d$ to get

$$\begin{aligned}\sum_{m=-\infty}^{\infty} \frac{2\sigma(\delta z_n - \delta z_m)}{(md)^3} &= C\mathrm{e}^{\mathrm{j}(knd-\omega t)} \sum_{m=1}^{\infty} \frac{2\sigma}{(md)^3}[1 - \mathrm{e}^{-\mathrm{j}kmd} - (1 - \mathrm{e}^{\mathrm{j}kmd})] \\ &= C\mathrm{e}^{\mathrm{j}(knd-\omega t)} \sum_{m=1}^{\infty} \frac{4\sigma}{(md)^3}\mathrm{j}\sin(kmd) \\ &= C\mathrm{e}^{\mathrm{j}(knd-\omega t)}\mathrm{j}\Omega,\end{aligned} \tag{15}$$

where Ω is given by

$$\Omega = \frac{4\sigma}{d^3} \sum_{m=1}^{\infty} \frac{\sin(kmd)}{m^3}, \tag{16}$$

One can readily verify using the Weierstrass M-test that the series $\sum_{m=1}^{\infty} \frac{\sin(m(kd))}{m^3}$ converges uniformly. We obtain an explicit expression for this sum using the Fourier series expansion of a cubic polynomial function [6, equation 1.443.5].

$$\Omega(k) = \frac{2\sigma}{d^3}\left[\frac{\pi^2}{3}(kd) - \frac{\pi}{2}(kd)^2\mathrm{sgn}(k) + \frac{1}{6}(kd)^3\right]. \tag{17}$$

Here, $\mathrm{sgn}(k)$ denotes the sign of k.

Details of Fourier series expansion. Back to (16), for $k > 0$, consider rewriting

$$\sum_{m=1}^{\infty} \frac{\sin(mkx)}{m^3} = A_0 x + B_0 x^2 + C_0 x^3. \tag{18}$$

Apply Fourier sine expansion to x, x^2 and x^3, with periodicity $L = \pi/k$ (note that if $x = d$, $L \geq d$, $kd \leq \pi$, agreeing with the relation for minimum wavenumber) to get

$$x = \sum_{m=1}^{\infty} A_m \sin(mkx), \quad x^2 = \sum_{m=1}^{\infty} B_m \sin(mkx), \quad x^3 = \sum_{m=1}^{\infty} C_m \sin(mkx).$$

where

$$\begin{aligned}A_m &= \frac{2k}{\pi}\int_0^{\pi/k} x\sin(mkx)dx = \frac{-2}{mk}(-1)^m, \\ B_m &= \frac{2k}{\pi}\int_0^{\pi/k} x^2\sin(mkx)dx = -\frac{4}{m^3k^2\pi} + \frac{4(-1)^m}{m^3k^2\pi} - \frac{2\pi(-1)^m}{k^2}, \\ C_m &= \frac{2k}{\pi}\int_0^{\pi/k} x^3\sin(mkx)dx = \frac{12(-1)^m}{m^3k^3} - \frac{2\pi^2(-1)^m}{mk^3}.\end{aligned} \tag{19}$$

Substitute into (18) and match the coefficients of the term of $(-1)^m/m$, $(-1)^m/m^2$, $1/m^3$ and on both sides of the resulting equation to get

$$\begin{aligned}\frac{2}{k}A_0 + \frac{2\pi}{k^2}B_0 + \frac{2\pi^2}{k^3}C_0 &= 0, \\ \frac{4}{k^3\pi}B_0 + \frac{12}{k^3}C_0 &= 0, \\ -\frac{4}{k^2\pi}B_0 &= 1.\end{aligned} \tag{20}$$

whose solution is given by

$$A_0 = \frac{\pi^2 k}{6}, \qquad B_0 = \frac{-\pi k^2}{4}, \qquad C_0 = \frac{k^3}{12}. \tag{21}$$

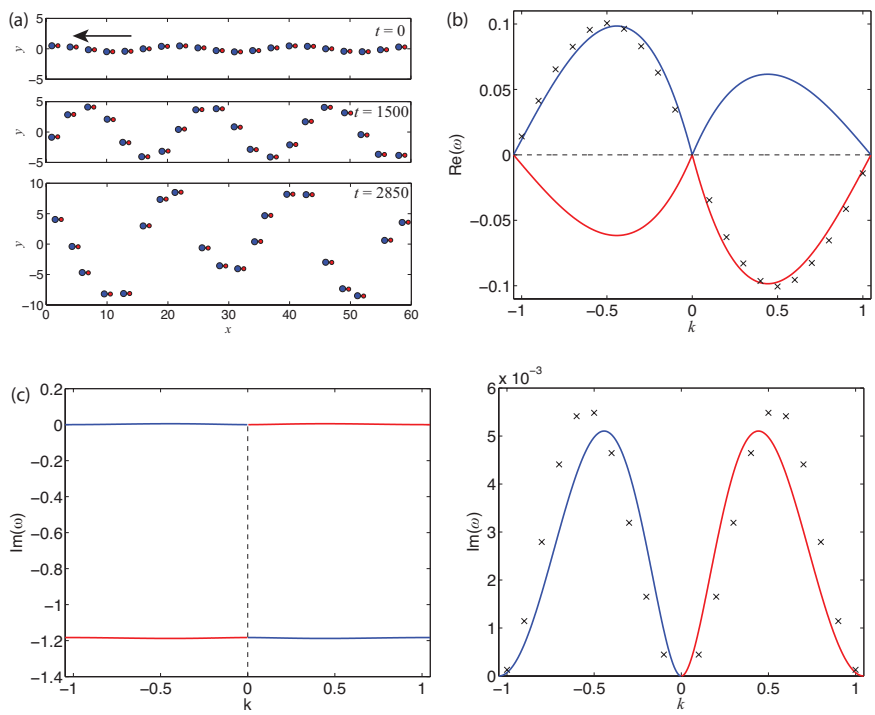

Figure 2: *Train of active particles: (a) Snapshots of a slowly growing transverse mode for $U = 1$, $V = 1$, $k = 3\pi/10$, $\mu = 0.5$, $\nu = 1$. The arrow indicate the directions of wave propagation. (b) Dispersion relation of the transverse mode for $U = 1$, $V = 1$. The blue and red lines corresponds to the two branches of the solution given by* (30)*. (c) Growth and decay rate of the two branches of solutions. The right panel magnifies the positive growth rate of the left panel. Analytical solutions are shown in solid lines and numerical results in $'\times'$ signs.*

For $k < 0$, follow the same analysis but with $x^2 = -\sum_{m=1}^{\infty} B_m \sin(mkx)$, this will give

$$A_0 = \frac{\pi^2 k}{6}, \qquad B_0 = \frac{\pi k^2}{4}, \qquad C_0 = \frac{k^3}{12}. \tag{22}$$

Set $x = d$ and substitute the above results to (16) give the closed form expression for Ω

$$\Omega = \frac{2\sigma}{d^3}\left[\frac{\pi^2}{3}(kd) - \frac{\pi}{2}(kd)^2 \mathrm{sgn}(k) + \frac{1}{6}(kd)^3\right]. \tag{23}$$

5 Dispersion relations

Lattice of passively-driven particles. Consider the case of passively-driven particles for which $U = 0$ and $\alpha_n = 0$ for all time. The translation motion in (14) becomes, upon substituting $\delta z_n = C\mathrm{e}^{\mathrm{i}(knd-\omega t)}$ and the expression in (15),

$$\overline{C}\omega = \mu C\Omega. \tag{24}$$

Therefore, for a purely longitudinal mode ($C = A$), the dispersion relation is $\omega = \mu\Omega$. For a purely transverse mode ($C = \mathrm{i}B$), the dispersion relation is $\omega = -\mu\Omega$, which is exactly opposite to the longitudinal mode.

Lattice of active particles. Now consider the case of active particles for which $U \neq 0$, the dispersion relation for the longitudinal mode ($C = A$) is linearly stable and takes exactly the same form as when $U = 0$, that is, $\omega = \mu\Omega$. However, the transverse mode ($C = \mathrm{i}B$) is qualitatively distinct from the case when $U = 0$, due to the instability arising from the activity and orientation dynamics of the active particles.

Here, it is instructive to rewrite (14) in matrix form by introducing $X_n = A\mathrm{e}^{\mathrm{j}(knd-\omega t)}$, $Y_n = B\mathrm{e}^{\mathrm{j}(knd-\omega t)}$ and $\Theta_n = \delta\alpha_n$,

$$\begin{pmatrix} \dot{X}_n \\ \dot{Y}_n \\ \dot{\Theta}_n \end{pmatrix} = \begin{pmatrix} -\mathrm{j}\mu\Omega & 0 & 0 \\ 0 & \mathrm{j}\mu\Omega & U \\ 0 & \mathrm{j}\nu\Omega & -\nu(V+u) \end{pmatrix} \begin{pmatrix} X_n \\ Y_n \\ \Theta_n \end{pmatrix} \tag{25}$$

Clearly, the longitudinal mode X_n decouples from the transverse mode Y_n and the orientational motion Θ_n; it is linearly stable. Meanwhile, the transverse mode and rotational motion are coupled at the linear order, yielding

$$\begin{aligned} \mathrm{j}\omega Y_n &= -U\Theta_n - \mathrm{j}\mu\Omega Y_n, \\ \dot{\Theta}_n &= -\nu(V+u)\Theta_n + \mathrm{j}\nu\Omega Y_n \end{aligned} \tag{26}$$

The orientation equation can be solved directly keeping in mind that $Y_n = B\mathrm{e}^{\mathrm{j}(knd-\omega t)}$ to get

$$\Theta_n = \frac{B\Omega\mathrm{j}\mathrm{e}^{\mathrm{j}knd}(\mathrm{e}^{-\mathrm{j}\omega t} - \mathrm{e}^{-\nu(V+u)t})}{-\mathrm{j}\omega + \nu(V+u)} \tag{27}$$

To obtain the dispersion relation, we neglect the transient term and substitute back into the first equation in (26). The translation equation then becomes

$$\mathrm{j}\omega = -\frac{\nu U\Omega\mathrm{j}}{-\mathrm{j}\omega + \nu(V+u)} - \mu\Omega\mathrm{j}, \tag{28}$$

which, upon further simplifications, gives

$$\omega^2 + [\nu(V+u)\mathrm{j} + \mu\Omega]\omega + \nu U\Omega\mathrm{j} + \mu\nu(V+u)\Omega\mathrm{j} = 0. \tag{29}$$

Solving (29) gives two solution branches,

$$\omega = \frac{1}{2}\left[-\nu(V+u)\mathrm{j} - \mu\Omega \pm \sqrt{(\nu(V+u)\mathrm{j} - \mu\Omega)^2 - 4\nu U\Omega\mathrm{j}}\right]. \tag{30}$$

The dispersion relation is given by the real part of ω, that is, the relation between the perturbation frequency $\mathrm{Re}\,[\omega]$ and wavenumber k. The growth rate of the perturbation is given by the imaginary part of ω. Depending on the sign of k, the two branches of ω correspond to either a slowly growing unstable mode or a fast decaying stable mode, see Fig. 2. Note that only the slowly growing unstable mode can be observed in forward-time numerical simulations. We refer to it as the dominant mode.

Limit of large background flow. Consider the strong flow limit, $V/U \gg 1$. In this case, one has $\sigma \approx -a^2(1-\mu)V$ and, thus, Ω and u are proportional to V. It is thus convenient to write

$$V + u = VP, \quad \text{and} \quad \Omega = VQ, \tag{31}$$

where

$$\begin{aligned} P &= 1 - \frac{\pi^2(1-\mu)}{3d^2}, \\ Q &= -\frac{2(1-\mu)a^2}{d^3}\left[\frac{\pi^2}{3}(kd) - \frac{\pi}{2}(kd)^2\mathrm{sgn}(k) + \frac{1}{6}(kd)^3\right]. \end{aligned} \tag{32}$$

That is, P is a positive parameter and $Q(k)$ is independent of V. The coupled transverse and rotational motion in (25) can be rewritten as

$$\begin{pmatrix} \dot{Y}_n \\ \dot{\Theta}_n \end{pmatrix} = \begin{pmatrix} \mathrm{j}\mu QV & U \\ \mathrm{j}\nu QV & -\nu PV \end{pmatrix} \begin{pmatrix} Y_n \\ \Theta_n \end{pmatrix} \tag{33}$$

Clearly, in the limit of large V, the transverse and rotational motion remain coupled. One can directly compute the eigenvalues of the matrix in (33) to find that there always exists an unstable solution. Alternatively, one can take the limit $V/U \to \infty$ of the explicit expression in (30) to get an equivalent result. Here, we present the latter approach. To this end, the square root term in (30) can then be approximated as

$$\begin{aligned}\sqrt{[\nu(V+u)\mathrm{j}-\mu\Omega]^2-4\nu U\Omega\mathrm{j}} &= \mathrm{sgn}(k)[\nu VP\mathrm{j}-\mu VQ]\sqrt{1-\frac{4\nu UVQ\mathrm{j}}{[\nu VP\mathrm{j}-\mu VQ]^2}} \\ &\approx \mathrm{sgn}(k)\,[\nu VP\mathrm{j}-\mu VQ]\left(1-\frac{2\nu UVQ\mathrm{j}}{[\nu VP\mathrm{j}-\mu VQ]^2}\right).\end{aligned} \tag{34}$$

Note that the square root $\sqrt{(\nu VP\mathrm{j}-\mu VQ)^2}$ has four branches, $\pm\nu VP\mathrm{j}\mp\mu VQ$. Here, the signum function $\mathrm{sgn}(\cdot)$ is used to select the two branches $(\nu VP\mathrm{j}-\mu VQ)$ or $-(\nu VP\mathrm{j}-\mu VQ)$. The two branches of solution for ω given by (30) become

$$\lim_{V/U\to\infty}\omega = \frac{1}{2}\left[-\nu PV\mathrm{j}-\mu QV \pm \left(\nu PV\mathrm{j}-\mu QV+\frac{2\nu UQ[\nu P+\mu Q\mathrm{j}]}{\nu^2P^2+\mu^2Q^2}\right)\right]. \tag{35}$$

Simplify the above expression to get that, for the unstable branch, there exists a limit on the growth rate of the perturbation that is independent of V,

$$\lim_{V/U\to\infty}\mathrm{Im}_j[\omega] = \frac{\nu\mu UQ^2}{\nu^2P^2+\mu^2Q^2}. \tag{36}$$

The corresponding dispersion relation for the dominant mode reduces to $\lim_{V/U\to\infty}\mathrm{Re}_j[\omega] = -\mu VQ = -\mu\Omega$, which takes the same form as when $U = 0$, but in contrast to the growth rate, the wave frequency in the strong flow limit is unbounded. Basically, the limit $V/U \to \infty$ does not converge to the case $U = 0$.

6 Numerical Simulations

In all simulations, we normalize a to 1, and we fix $d = 3$. In the case of active particles ($U \neq 0$), we normalize $U = 1$. We compare the dispersion relation and growth rate obtained from the analytical solutions in the small perturbation limit to those obtained from numerical simulations of the full nonlinear equations (9) and (11). In the numerical simulations, we give the system an initial perturbation in the form of a sinusoidal wave with wavenumber $k = 2\pi M/(Nd)$. Here, M is the number of wave numbers in the periodic domain L. We vary the number of active particles N in the system to obtain the desired value of k and M, while keeping L/d in integer ratio to satisfy the periodic boundary conditions of the lattice.

We compute the numerical dispersion relation using discrete Fourier transform (DFT) of the numerical solutions. The wave frequency ω and wavenumber k of the perturbation are determined by the location of the sharp peak of the power spectrum. Details of the DFT implementation can be found in [7] and are omitted here for brevity. To ensure that our simulations are accurate enough to capture the correct wave frequency and growth rate for a particular k, we consider at least 10 wave cycles both spatially and temporally. Moreover, for the unstable transverse mode, we use a small amplitude perturbation ($B \sim 10^{-8}$) such that we can get longer sampling time for the wave frequency obtained from DFT before the nonlinear instability comes into play. To determine numerically the growth rate for a given k, we measure the maximum displacement of all active particles and the corresponding occuring time in each cycle, and then we average the growth rate over several cycles, with the numerical growth rate in individual cycle determined using the formula,

$$\mathrm{Im}_j[\omega]\big|_{\mathrm{numerical}} = \sum_{n=1}^{N}\frac{1}{N}\frac{\log(y_{n,max}(t_{max}+T)-y_{n,max}(t_{max}))}{T}. \tag{37}$$

where $y_{n,max}$ denotes the maximum amplitude of the n-th active particle, and t_{max} and $t_{max}+T$ denote the occuring time of the maximum amplitudes in the cycle.

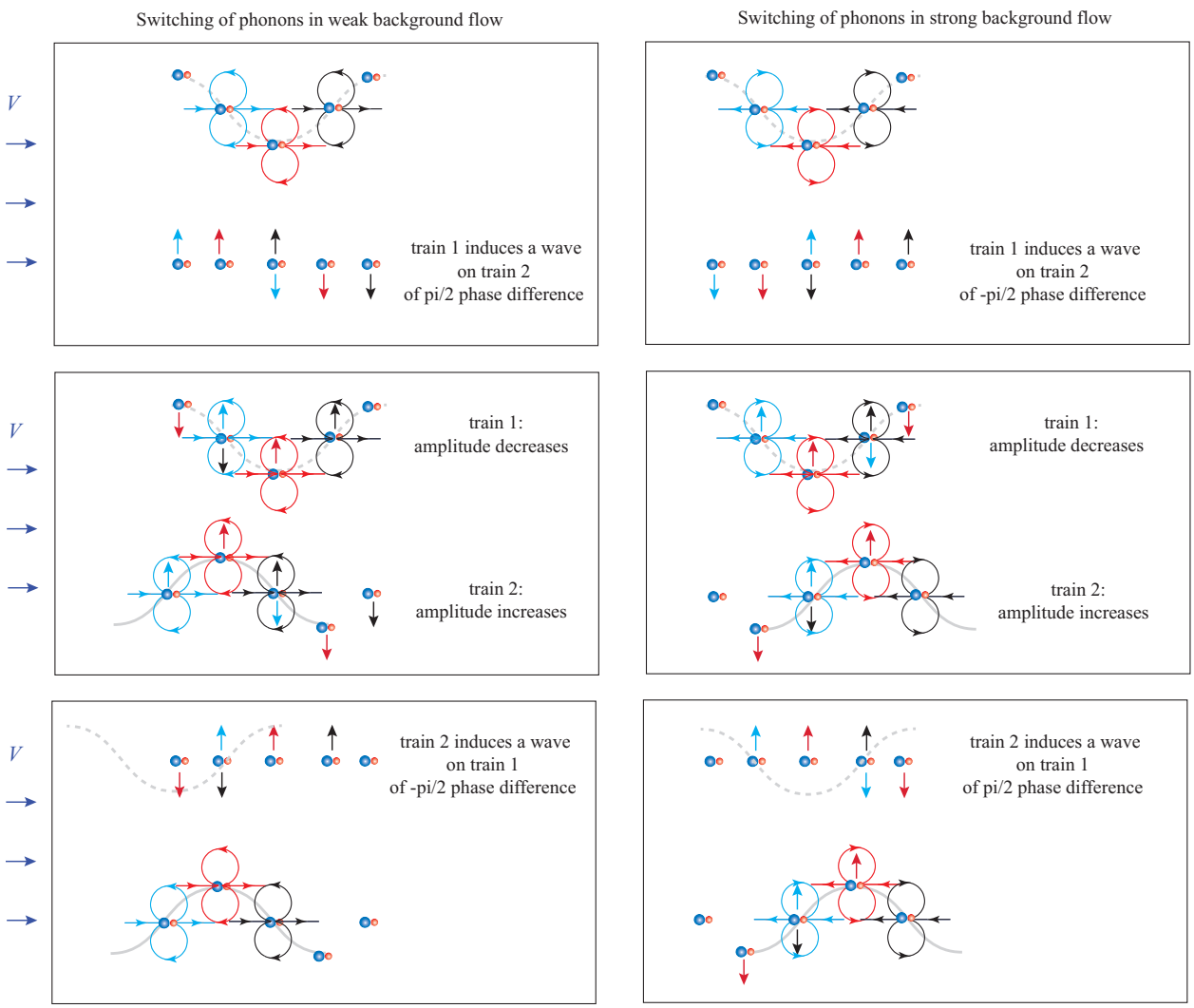

Figure 3: *Schematic depicting the hydrodynamic-based mechanism for the switching of phonons in weak and strong background flows.*

7 Switching of phonons

We observe a new phenomenon of phonon propagation in microfluidic lattices, which we term "switching", when we consider the wave-wave interaction of two adjacent trains separated by a distance of b. That is, the wave in one train switches back and forth between the two trains, mediated by the hydrodynamic interactions among the particles in the two trains. This switching pheomenon is observed in both driven and active particles, and can be explained by the dipolar nature of the flow filed induced by the particles (see Fig. 3). The switching frequency is an increasing function for σ, but a decreasing function for b.

The switching of phonon in passively-driven particles is stable for small amplitude perturbation for both longitudinal and transverse mode. However, the switching induces an instability in the lattices when the wave amplitude is large and b is small (See Movies 5 and 6). For the transverse mode, the nonlinear instability due to large amplitude perturbation is not surprising as this instability has been observed for phonon in one single train. But the instability in longitudinal mode, which is stable both linearly and nonlinearly in one train, is not obvious. The reason for this instability is as follow. The switching of two longitudinal modes of large perturbation can induce transverse modes of the same wave frequency as the longitudinal modes in both trains. The mode coupling of the induced transverse modes and the longitudinal

modes cause the instability of the lattices.

The switching of phonon in active particles is always unstable, for both longitudinal and transverse modes, small and large amplitude perturbations (See Movies 7 and 8). Switching does not induce any additional instability for the transverse phonon at the linear level, which has been verified by comparison of the numerical growth rate for the switching phonons and the transverse phonon in one train. However, when the amplitude of the transverse modes in the two trains increase, the interactions among the two adjacent trains become vigorous, and the lattices break eventually when the two waves collide. The switching of longitudinal modes induces the unstable transverse modes and, thus, are unstable.

8 Caption of the supplementary movies

In all movies, the coupled orientation and translation equations in (9) are evolved in time.

Movie 1: Single train of passively-driven particles in microfluidic channel – Longitudinal mode. Parameters values are $U = 0$, $V = 1$, $A = 0.5$, $k = \pi/5d$.

Movie 2: Single train of passively-driven particles in microfluidic channel – Transverse mode. Parameters values are $U = 0$, $V = 1$, $A = 0.5$, $k = \pi/5d$.

Movie 3: Single train of active particles in microfluidic channel – Longitudinal mode. Parameters values are $U = 1$, $V = 1.2$, $A = 0.5$, $k = \pi/5d$.

Movie 4: Single train of active particles in microfluidic channel – Transverse mode. Parameters values are $U = 1$, $V = 1.2$, $A = 0.5$, $k = \pi/5d$. Note that the change in orientation is of the order 0.1 radians and is therefore barely visible. However, this small reorienation is sufficient to trigger the coupling between the translational and rotational equations and kick off the slowly-growing instability of the lattice.

Movie 5: Two trains of passively-driven particles in microfluidic channel – Longitudinal mode: switching of waves and wave instabilities. Parameters values are $U = 0$, $V = 1$, $A = 0.5$, $b = 6$, $k = 0$ for the upper train and $k = 3\pi/10d$ for the lower train.

Movie 6: Two trains of passively-driven particles in microfluidic channel – Transverse mode: switching of waves and wave instabilities. Parameters values are $U = 0$, $V = 1$, $A = 0.5$, $b = 6$, $k = 0$ for the upper train and $k = \pi/2d$ for the lower train.

Movie 7: Two trains of active particles in microfluidic channel – Longitudinal mode: switching of waves and wave instabilities. Parameters values are $U = 1$, $V = 1.2$, $A = 0.5$, $b = 6$, $k = 0$ for the upper train and $k = \pi/5d$ for the lower train.

Movie 8: Two trains of active particles in microfluidic channel – Transverse mode: switching of waves and wave instabilities. Parameters values are $U = 1$, $V = 1.2$, $A = 0.5$, $b = 6$, $k = 0$ for the upper train and $k = \pi/5d$ for the lower train.

References

[1] S. Kim and S. J. Karrila. *Microhydrodynamics: principles and selected applications*. Courier Corporation, 2013.

[2] N. Liron and S. Mochon. Stokes flow for a stokeslet between two parallel flat plates. *Journal of Engineering Mathematics*, 10(4):287–303, 1976.

[3] E. Kanso and S. Michelin. Confined autophoretic particles. In preparation, 2018.

[4] T. Brotto, J.-B. Caussin, E. Lauga, and D. Bartolo. Hydrodynamics of confined active fluids. *Physical Review Letters*, 110(3):038101, 2013.

[5] A. C. H. Tsang. *Transitions in the Collective Behavior of Microswimmers Confined to Microfluidic Chips, PhD thesis*. University of Southern California, 2016.

[6] S. Gradshteyni and I. M. Ryzhik. *Tables of Integrals, Series, and Products. Corrected and enlarged edition*. Academic, 1980.

[7] T. Beatus, T. Tlusty, and R. Bar-Ziv. Phonons in a one-dimensional microfluidic crystal. *Nature Physics*, 2(11):743–748, 2006.